SINC Refocusing Pulses Given the severe nonlinearity of the Bloch equations for RF excitation with flip angles greater than 90° (see Section 3.1), it is somewhat surprising that SINC pulses can make effective refocusing pulses. (Refocusing pulses are normally played at a flip angle of 180°, but reduced flip angles, e.g., 130°, are sometimes used when SAR is a limiting factor, as discussed in Section 3.3.)

One reason that SINC pulses can be effectively used for refocusing pulses is that they are typically played with accompanying crusher gradients (see Section 10.2). It can be shown that the slice profile of a refocusing pulse with crushers is equal to the square of the small flip angle profile, which can be demonstrated with SLR analysis (Section 2.3). (Recall that the profile obtained at small flip angles is well approximated by the Fourier transform of the RF envelope and therefore does not contain nonlinearity introduced by the Bloch equations.) Figure 2.4 shows the responses of a SINC pulse with a 120° flip angle played as an excitation pulse and as a refocusing pulse (with crushers). Both responses were calculated with forward SLR transforms. The lack of side lobes in the refocusing pulse profile is a general result for this pulse and is valid even at a flip angle of 180°, as long as crushers accompany the pulse. Generally the effect of squaring any slice profile is to make it more sharply peaked, to suppress its side lobes, and to narrow it. Therefore, if SINC pulses that are identical (except in flip angle) are used for both excitation and refocusing in a spin echo pulse sequence, the amplitude of the slice-selection gradient of the refocusing SINC pulse is reduced by 25–40% to counteract the slice narrowing effect.

Table 2.2 gives some quantitative examples of the slice narrowing. When played as a small flip angle pulse ($\theta = 30°$), the values are nearly equal to unity, indicating that Eq. (2.3) holds to an excellent approximation. At $\theta = 90°$ the approximation is less accurate. When the SINC pulses are played as refocusing pulses, with crushers, the bandwidth is substantially lower, so that the amplitude of the slice-selection gradient must be reduced to obtain the expected slice thickness.

TABLE 2.2
RF Bandwidth[a], as Measured by the FWHM of the Slice Profile, for Two SINC Pulses Apodized with a Hamming Window

$\Delta f \times t_0$	$\theta = 30°$	$\theta = 90°$	$\theta = 180°$[b]
$N_L = N_R = N = 2$	1.01	1.09	0.67
$N_L = N_R = N = 4$	1.00	1.02	0.70

[a] In units of $1/t_0$. See Eq. (2.6).
[b] Refocus (with crushers).

SELECTED REFERENCES

MacFall, J. R., Charles, H. C., and Prost, R. 1990. Truncated SINC slice excitation for ^{31}P spectroscopic imaging. *Magn. Reson. Imaging* 8: 619–624.

Runge, V. M., Wood, M. L., Kaufman, D. M., and Silver, M. S. 1988. MR imaging section profile optimization: Improved contrast and detection of lesions. *Radiology* 167: 831–834.

RELATED SECTIONS

Section 3.1 Excitation Pulses
Section 3.3 Refocusing Pulses
Section 2.3 SLR Pulses

2.3 SLR Pulses

Given a slice-selective RF pulse and the initial orientation of the magnetization vector, the slice profile can be determined by solving the Bloch equations for M_x, M_y, and M_z (e.g., see Eq. 3.13 in Chapter 3). Although numerical methods are usually required, the process is straightforward and deterministic. The inverse problem, however, is much more difficult. Given the desired slice profile and the initial condition of the magnetization, what RF pulse should be applied? For small flip angles, the shape of an excitation pulse can be determined (to an excellent approximation) by inverse Fourier transformation of the slice profile (Section 3.1). This procedure begins to fail for pulses with larger flip angles (i.e., over the range 30–90°) due to the nonlinearity of the Bloch equations. In those cases, the RF pulse can be determined by iterative numerical optimization methods (for example, using optimal control theory), but this process is time-consuming and has limited flexibility for making trade-offs among pulse parameters. A summary of iterative and other RF pulse design methods can be found in Warren and Silver (1988, chap. 4).

The Shinnar–Le Roux (SLR) algorithm (Le Roux 1986; Shinnar, Eleff, et al. 1989; Shinnar, Bolinger, et al. 1989a, 1989b; Shinnar and Leigh 1989; Pauly et al. 1991) allows this inverse problem to be solved directly and efficiently, without iteration. Characteristics such as RF bandwidth, pulse duration, flip angle, percent ripple in the passband, and percent ripple in the stopband are specified, and the algorithm returns the exact RF pulse through a straightforward computational process. Moreover, the SLR algorithm allows the pulse designer to make trade-offs among these parameters before the pulse is even generated. Because of these advantages, the SLR algorithm has found widespread use for nonadiabatic pulse design in imaging and spectroscopy.

The SLR algorithm uses two key concepts: the two-dimensional mathematical representation of rotations known as SU(2), and the hard pulse

approximation. Rotations in three-dimensional space can be described equally well by two distinct representations. The first representation uses the familiar 3×3 orthogonal rotation matrices and 3×1 vectors. This set of 3×3 rotation matrices is said to be the special orthogonal 3D group, or SO(3). The second representation uses 2×2 unitary matrices, and 2×1 complex vectors called *spinors* (Le Roux 1986; Shinnar and Leigh 1989; Pauly et al. 1991). The set of rotation 2×2 unitary matrices is said to be the special unitary 2D group, or SU(2). Both the SO(3) and SU(2) representations are equally valid to describe macroscopic rotations such as those experienced by the magnetization vector. The SU(2) representation for rotations is used in the SLR algorithm because it offers considerable mathematical simplification.

The second key concept of the SLR algorithm is the hard pulse approximation (Le Roux 1986; Shinnar, Eleff, et al. 1989), which is useful for nonadiabatic pulses and is depicted in Figure 2.5. The hard pulse approximation states that any shaped, or soft, pulse $B_1(t)$ can be approximated by a series of short hard pulses separated by periods of free precession. The approximation becomes progressively more accurate as the number of hard pulses increases and the duration of the free precession periods decreases. When rotations are described in the SU(2) representation and the hard pulse approximation is used, the effect of any soft pulse on the magnetization can be mathematically described by two polynomials with complex coefficients. The process that transforms from the RF pulse to the two polynomials is called the *forward SLR transform*. It is important that the *inverse SLR transform* also can be calculated. The inverse transform yields the RF pulse, given the two complex polynomials corresponding to the desired magnetization.

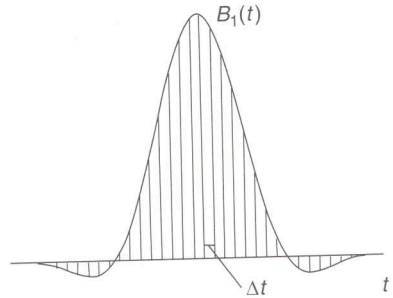

FIGURE 2.5 The hard pulse approximation. A selective or 'soft' RF pulse $B_1(t)$ can be approximated by a series of hard pulses, represented by the vertical lines. The hard pulses are separated by periods of free precession of duration Δt. As the number of hard pulses increases and Δt decreases, the accuracy of the hard pulse approximation improves.

In digital signal processing (DSP), these polynomials are filters for which there are well-established and powerful design tools available. In the SLR algorithm, the inverse SLR transform is used in conjunction with finite impulse response (FIR) filter design tools to design RF pulses directly (Shinnar, Bolinger, et al. 1989b; Pauly et al. 1991).

This section introduces the reader to the main concepts underlying the SLR algorithm. If the reader wants to actively engage in SLR pulse design, additional details beyond the scope of this section will be required and the reader is referred to Pauly et al. (1991) the DSP references therein. Several excellent commercial and shareware software packages for FIR filter design are also available. (We cannot recommend any particular package here, but if the reader enters key words such as *filter design*, *Remez*, and *Parks-McClellan* into an Internet search engine, several options will appear.)

2.3.1 MATHEMATICAL DESCRIPTION

Rotations Rotations in three dimensions can be described equivalently by either the SO(3) or SU(2) representations. In the SO(3) representation, the familiar 3×3 rotation matrices have nine real matrix elements. The matrices are orthogonal and normalized (often called orthonormal):

$$\Re\Re^T = \Re^T\Re = \mathbb{I} \tag{2.7}$$

where $\Re^T$ represents the transpose of the matrix $\Re$ and $\mathbb{I}$ is the identity matrix. Because a general rotation can be completely specified by three free parameters (e.g., three Euler angles χ, ψ, and η), Eq. (2.7) represents $9 - 3 = 6$ constraints.

In the SU(2) representation, a general rotation matrix $\mathbb{Q}$ can be written:

$$\mathbb{Q} = \begin{bmatrix} \alpha & -\beta^* \\ \beta & \alpha^* \end{bmatrix} \tag{2.8}$$

where α and β are complex numbers known as the Cayley-Klein parameters and the asterisk represents complex conjugation. The matrix $\mathbb{Q}$ is unitary; that is:

$$\mathbb{Q}\mathbb{Q}^\dagger = \mathbb{Q}^\dagger\mathbb{Q} = \mathbb{I} \tag{2.9}$$

where $\mathbb{Q}^\dagger$ is the Hermitian conjugate or adjoint of $\mathbb{Q}$, which is obtained by transposing $\mathbb{Q}$ and taking the complex conjugate of each element. Note the product of unitary matrices is also a unitary matrix. Because the two complex Cayley-Klein parameters α and β contain a total of four real numbers, Eq. (2.9) contains only $4 - 3 = 1$ constraint. (Again recall that three free parameters are

required to describe a general rotation.) From Eqs. (2.8) and (2.9), that single constraint is the normalization condition:

$$\alpha\alpha^* + \beta\beta^* = |\alpha|^2 + |\beta|^2 = 1 \tag{2.10}$$

The rotation matrix $\mathbb{Q}$ acts on 2×1 complex vectors (i.e., the spinors). In the SLR algorithm, the initial state of the spinor is taken to be:

$$s_0 = \begin{bmatrix} 1 \\ 0 \end{bmatrix} \tag{2.11}$$

Note that the effect of the unitary rotation matrix in Eq. (2.8) on the initial state of the spinor is

$$\mathbb{Q}s_0 = \begin{bmatrix} \alpha \\ \beta \end{bmatrix} \tag{2.12}$$

In other words the elements of the spinor are the Cayley-Klein parameters. Thus, the elements of the spinor satisfy the same normalization constraint that is given in Eq. (2.10).

The mathematical simplification afforded by the SU(2) representation is a consequence of the fewer number of constraints implicit in Eq. (2.9) versus Eq. (2.7) (i.e., one versus six). This situation is analogous to solving a system of linear equations, where it is nearly always easier to solve fewer equations with fewer constraints.

Given three Euler angles χ, ψ, and η, a two-dimensional unitary matrix can be written for the rotation (Goldstein 1980, Chap. 4):

$$\mathbb{Q} = \begin{bmatrix} e^{i(\chi+\psi)/2}\cos\dfrac{\eta}{2} & ie^{-i(\chi-\psi)/2}\sin\dfrac{\eta}{2} \\ ie^{i(\chi-\psi)/2}\sin\dfrac{\eta}{2} & e^{-i(\chi+\psi)/2}\cos\dfrac{\eta}{2} \end{bmatrix} \tag{2.13}$$

Note the appearance of the half values of the angles in Eq. (2.13), which is typical in the SU(2) representation. A rotation by 2π (i.e., $\eta \rightarrow \eta + 2\pi$) negates the matrix $\mathbb{Q}$, whereas the same rotation leaves the corresponding 3×3 orthogonal rotation matrix $\Re$ unchanged. Thus there is a one-to-one correspondence between elements of SO(3) and SU(2), that is, between $\Re$ and the pair $(-\mathbb{Q}, \mathbb{Q})$.

Although the SU(2) representation offers some mathematical simplification, ultimately the rotation of the magnetization vector occurs in real, three-dimensional space. A set of rules, or dictionary, that translates between the SU(2) and the SO(3) representations is required. Those rules were given

by Jaynes (1955) and later adapted in Pauly et al. (1991). Defining the complex transverse magnetization in terms of the x and y components of the magnetization vector:

$$\begin{aligned} M_\perp &= M_x + iM_y \\ M_\perp^* &= M_x - iM_y \end{aligned} \tag{2.14}$$

the magnetization before $(-)$ and after $(+)$ a rotation is given by:

$$\begin{bmatrix} M_\perp(+) \\ M_\perp^*(+) \\ M_z(+) \end{bmatrix} = \begin{bmatrix} (\alpha^*)^2 & -\beta^2 & 2\alpha^*\beta \\ -(\beta^*)^2 & \alpha^2 & 2\alpha\beta^* \\ -(\alpha\beta)^* & -\alpha\beta & \alpha\alpha^* - \beta\beta^* \end{bmatrix} \begin{bmatrix} M_\perp(-) \\ M_\perp^*(-) \\ M_z(-) \end{bmatrix} \tag{2.15}$$

where α and β are the Cayley-Klein parameters. Several important special cases (Pauly et al. 1991) can be extracted from Equation (2.15). For example, consider an inversion pulse. Prior to the application of the pulse, assume the magnetization is entirely aligned with the z axis and is assumed to have its maximal equilibrium value:

$$\begin{aligned} M_\perp(-) &= 0 \\ M_z(-) &= M_0 \end{aligned} \tag{2.16}$$

Substituting Eq. (2.16) into Eq. (2.15), and applying the normalization condition of Eq. (2.10) yields:

$$M_z(+) = M_0(\alpha\alpha^* - \beta\beta^*) = M_0(1 - 2|\beta|^2) \tag{2.17}$$

Note that the expression for the inversion slice profile in Eq. (2.17) is a real quantity, as it must be, even though the individual Cayley-Klein parameters are complex numbers. Table 2.3 gives several other special cases.

The Hard Pulse Approximation and the Forward SLR Transform This subsection gives an overview of the hard pulse approximation and forward SLR transform. For more details, the reader is referred to Pauly et al. (1991); here we mainly follow the notation of that paper.

Recall that a selective, or soft, pulse can be approximated by a series of hard pulses, separated by periods of free precession (Fig. 2.5). In this way the net effect of the RF pulse can be approximated by a series of nutations and free precessions. Each nutation and each precession produces a rotation of the magnetization vector, which can be described by a unitary rotation matrix in the SU(2) representation. If relaxation effects are ignored, the net effect of all the nutations and precessions is a composite rotation that can be described by a

TABLE 2.3
Response of the Magnetization to Commonly used RF Pulse Types in Terms of the Cayley-Klein Parameters

Pulse Type	Initial Condition (M_x, M_y, M_z)	Final State
Excitation or saturation	$(0, 0, M_0)$	$M_x = 2M_0\mathrm{Re}(\alpha\beta^*)$ $M_y = 2M_0\mathrm{Im}(\alpha\beta^*)$ $M_\perp = 2\alpha\beta^*$
Inversion	$(0, 0, M_0)$	$M_z = M_0(1 - 2\lvert\beta\rvert^2)$
Refocus (without crushers)	$(0, M_0, 0)$	$M_\perp = iM_0((\alpha^*)^2 + \beta^2)$
Refocus (with crushers, which dephase the $(\alpha^*)^2$ term giving a voxel average of 0)	$(0, M_0, 0)$	$M_\perp = iM_0\beta^2$

single unitary matrix obtained by multiplying the individual rotation matrices in sequence.

As shown in Figure 2.5, the hard pulses are taken to be a series of spikes (i.e., delta functions) with adjacent hard pulses separated by a time interval Δt. So that the entire series of hard pulses produces the same flip angle as the soft pulse, the incremental flip angle produced by the jth hard pulse must be

$$\theta_j = \gamma |B_{1,j}| \Delta t \tag{2.18}$$

(Equation 2.18 can be interpreted as approximating the integral under the soft pulse by a series of rectangles.) The SLR algorithm does not require the RF field to lie along a single direction in the rotating frame, so $B_{1,j}$ is represented by a complex value, as discussed in Section 1.2 (hence the absolute value in Eq. 2.18). If the phase of the RF field in the rotating frame is given by:

$$\varphi_j = \measuredangle(B_{1,j}) = \arg(B_{1,j}), \tag{2.19}$$

then, θ_j and φ_j are related to the three Euler angles by $\eta = \theta_j$, $\chi = -\psi$ and $\chi - \psi = 2\varphi_j$. The rationale behind choosing these values for the Euler angles is explained in Figure 2.6. Equation (2.13) then provides the unitary matrix that describes the jth nutation:

$$\mathbb{Q}_{\text{nutation},j} = \begin{bmatrix} \cos\dfrac{\theta_j}{2} & ie^{-i\varphi_j}\sin\dfrac{\theta_j}{2} \\ ie^{i\varphi_j}\sin\dfrac{\theta_j}{2} & \cos\dfrac{\theta_j}{2} \end{bmatrix} \tag{2.20}$$

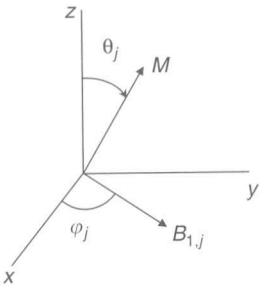

FIGURE 2.6 Nutation of the magnetization by the jth hard pulse. Because $B_{1,j}$ can be complex (i.e., can make any angle φ_j with respect to the x axis in the rotating frame) the nutation is described by three Euler angles. First, a rotation about z by the Euler angle $\psi = -\varphi_j$ aligns $B_{1,j}$ with the x axis. Then, a rotation about the x axis by $\eta = \theta_j$ accomplishes the nutation. Finally, $B_{1,j}$ is restored to its initial orientation with a rotation about the z axis by $\chi = +\varphi_j$.

Again using Eq. (2.13), and assuming both Δt and the resonant offset ω to be independent of the index j, the unitary rotation matrix describing any precession period is obtained by setting $\eta = \chi = 0$ and ψ equal to the precession angle:

$$\mathbb{Q}_{\text{precession}} = \begin{bmatrix} e^{i\psi/2} & 0 \\ 0 & e^{-i\psi/2} \end{bmatrix} = \begin{bmatrix} z^{1/2} & 0 \\ 0 & z^{-1/2} \end{bmatrix} = z^{1/2}\begin{bmatrix} 1 & 0 \\ 0 & z^{-1} \end{bmatrix} \tag{2.21}$$

The variable z is related to the resonant offset, which is determined by the gradient $\vec{G}$ and displacement $\vec{r}$ from isocenter:

$$z = \exp(i\psi) = \exp(i\omega\Delta t) = \exp(i2\pi f\Delta t) = \exp(i\gamma\vec{G}\cdot\vec{r}\Delta t) \tag{2.22}$$

(For spectrally selective pulses in Section 4.3, there is no slice-selection gradient, so the last term of Eq. 2.22 does not apply.) If, without loss of generality, it is assumed that the free precession precedes the nutation, then the effect of the first precession and nutation on the initial state given in Eq. (2.11) is:

$$\begin{aligned} s_1 = \mathbb{Q}_{\text{nutation},1}\mathbb{Q}_{\text{precession}}s_0 &= z^{1/2}\begin{bmatrix} \cos\dfrac{\theta_1}{2} & ie^{-i\varphi_1}\sin\dfrac{\theta_1}{2} \\ ie^{i\varphi_1}\sin\dfrac{\theta_1}{2} & \cos\dfrac{\theta_1}{2} \end{bmatrix}\begin{bmatrix} 1 & 0 \\ 0 & z^{-1} \end{bmatrix}\begin{bmatrix} 1 \\ 0 \end{bmatrix} \\ &= z^{1/2}\begin{bmatrix} \cos\dfrac{\theta_1}{2} \\ ie^{i\varphi_1}\sin\dfrac{\theta_1}{2} \end{bmatrix} \equiv z^{1/2}\begin{bmatrix} C_1 \\ S_1 \end{bmatrix} \end{aligned} \tag{2.23}$$

Equation (2.23) contains the definition of C_1 and S_1, and C_j and S_j are defined analogously. The spinor state after the jth precession can be obtained by recursion:

$$s_j = \mathbb{Q}_{\text{nutation},j}\mathbb{Q}_{\text{precession}}s_{j-1} \tag{2.24}$$

For example,

$$\begin{aligned} s_2 &= \mathbb{Q}_{\text{nutation},2}\mathbb{Q}_{\text{precession}}s_1 \\ &= z\begin{bmatrix} \cos\frac{\theta_2}{2} & ie^{-i\varphi_2}\sin\frac{\theta_2}{2} \\ ie^{i\varphi_2}\sin\frac{\theta_2}{2} & \cos\frac{\theta_2}{2} \end{bmatrix}\begin{bmatrix} 1 & 0 \\ 0 & z^{-1} \end{bmatrix}\begin{bmatrix} \cos\frac{\theta_1}{2} \\ ie^{i\varphi_1}\sin\frac{\theta_1}{2} \end{bmatrix} \\ &= z\begin{bmatrix} C_2C_1 - S_1S_2^*z^{-1} \\ C_1S_2 + S_1C_2z^{-1} \end{bmatrix} \end{aligned} \tag{2.25}$$

Defining the jth spinor state in terms of two complex polynomials:

$$s_j = z^{j/2}\begin{bmatrix} A_j(z) \\ B_j(z) \end{bmatrix} \tag{2.26}$$

it can be seen from Eqs. (2.24) and (2.25) that $A_j(z)$ and $B_j(z)$ are each polynomials of order $j-1$ in the variable z^{-1}. After the entire RF pulse has been approximated by N interleaved periods of free precession and hard pulses, we have:

$$s_N = z^{N/2}\begin{bmatrix} A_N(z) \\ B_N(z) \end{bmatrix} \tag{2.27}$$

Note that from Eq. (2.25), the constant term in the polynomial A_N is a product of the cosine terms:

$$A_{N,0} = C_NC_{N-1}C_{N-2}\cdots C_2C_1 \tag{2.28}$$

All of the other terms in the polynomial A_N contain at least one factor of S_j, each of which is proportional to $\sin(\theta_j/2)$ and hence proportional to θ_j (because $\theta_j \ll 1$ rad). For small flip angles, all those terms are negligible in comparison to the constant term, so

$$A_N(z) \approx A_{N,0} = C_NC_{N-1}C_{N-2}\cdots C_2C_1 \approx 1 \tag{2.29}$$

because C_j is equal to $\cos\left(\frac{\theta_j}{2}\right) \approx 1$.

From Eqs. (2.12) and (2.27), the two polynomials A_N and B_N are related to the Cayley-Klein parameters for the net rotation by:

$$\begin{aligned} A_N(z) &= z^{-N/2}\alpha \\ B_N(z) &= z^{-N/2}\beta \end{aligned} \tag{2.30}$$

According to Eq. (2.22), $|z| = 1$, so the polynomials A_N and B_N satisfy the normalization constraint:

$$|A_N(z)|^2 + |B_N(z)|^2 = 1 \tag{2.31}$$

At this point, we have demonstrated the forward SLR transform from the RF pulse to the two polynomials in Eq. (2.27). The resulting magnetization is found from Eq. (2.30) and the relationships in Table 2.3.

Equation (2.29) provides further insight when used to interpret Table 2.3. For example, small flip angle excitation pulses satisfy $|\alpha| \approx 1$ because the cosines of all the hard pulse flip angles are approximately 1, and the sines are approximately 0. Because the small flip angle response is approximately proportional to the Fourier transform of the pulse, we can infer that $|\alpha\beta^*| \approx |\beta^*| = |\beta|$ must also be proportional to the magnitude of the Fourier transform of $B_1(t)$. Examining the result for the refocusing pulse (with crushers), we see that its slice profile is related to the square of the small flip angle excitation slice profile. This explains, for example, the narrowing of the slice profile of a SINC pulse used as a refocusing pulse (with crushers) compared to one used as an excitation pulse (Section 2.2).

The Inverse SLR Transform The inverse SLR transform translates from the two polynomials $A_N(z)$ and $B_N(z)$ back to the jth RF pulse element $B_{1,j}$. Like the forward SLR transform, the inverse is calculated recursively. Inverting Eq. (2.24), and recalling the unitary property of the matrices (i.e., Eq. 2.9) yields:

$$\begin{aligned} s_{j-1} = z^{(j-1)/2}\begin{bmatrix} A_{j-1}(z) \\ B_{j-1}(z) \end{bmatrix} &= \mathbb{Q}^{-1}_{\text{precession}}\mathbb{Q}^{-1}_{\text{nutation},j}\,s_j \\ &= \mathbb{Q}^{\dagger}_{\text{precession}}\mathbb{Q}^{\dagger}_{\text{nutation},j}\,s_j \end{aligned} \tag{2.32}$$

Because $A_j(z)$ and $B_j(z)$ are polynomials of order $j-1$ in z^{-1}, the constraint that their orders must decrease by one power of z^{-1} for each iteration provides sufficient information to calculate their coefficients. As described in detail in Pauly et al. (1991), that constraint allows the amplitude and phase of the hard

pulse $B_{1,j}$ to be calculated with the relationship:

$$\gamma|B_{1,j}|\Delta t = 2\arctan\left|\frac{B_{j,0}}{A_{j,0}}\right|$$
$$\measuredangle(B_{1,j}) = \measuredangle\left(-i\frac{B_{j,0}}{A_{j,0}}\right) \tag{2.33}$$

where $A_{j,0}$, and $B_{j,0}$ are the lowest order (i.e., constant) terms of the polynomials $A_j(z)$ and $B_j(z)$ (note that on the left-hand side of Eq. (2.33) $B_{1,j}$ is the RF field strength, not to be confused with the polynomial B.) By proceeding with the recursion, the entire hard pulse approximation can be recovered from the polynomials A and B. This provides the inverse SLR transform.

In practical calculations, for computational efficiency N is usually taken to be less than the number of the digital points used to ultimately represent the RF pulse on the MRI scanner. The final high-resolution digital representation of the pulse is obtained with interpolation (e.g., with cubic splines) of the hard pulse representation. If N is chosen too small, the hard pulse approximation begins to break down. Typically, N might be chosen to be 20–100, while the final digital resolution of the pulse can be 100–1000 or more, depending on its duration and on the details of the digital-to-analog converter (DAC) in the RF chain.

The Polynomials A and B To design an RF pulse, the filter (i.e., polynomial) $B_N(z)$ is matched to the desired frequency response. This is done by a procedure described in Le Roux (1986) and Pauly et al. (1991) and outlined next. From Eqs. (2.8) and (2.13), we note that $|\beta| = |B_N| = \sin(\eta/2)$ where η is the net nutation angle of the pulse. First we generate up an ideal $B_N(z)$ polynomial that is equal to the sine of one-half the desired flip angle of the ideal profile. (Recall that z is related to the spatial coordinates by Eq. 2.22.) For example, to design a 90° pulse we set the ideal $B_N(z)$ equal to 0 in the stopband and equal to the constant value:

$$\sin\left(\frac{90°}{2}\right) \approx 0.707 \tag{2.34}$$

in the passband. This ideal slice profile cannot be realized with a finite-length RF pulse, so a more realistic profile with a finite transition band and ripples is used instead. We can generate the realistic polynomial with the Parks-McClellan algorithm (Oppenheim and Schaeffer 1975, Chap. 5), which is also sometimes referred to as the Remez exchange algorithm. Figure 2.8a (later in this chapter) shows an example of the resulting $B_N(z)$ polynomial. Note that

the finite-width transition band, the passband ripples, and the amplitude in the passband (~0.7) are consistent with Eq. (2.34).

To perform the inverse SLR transform we also need to determine the polynomial $A_N(z)$. There are many possible choices that satisfy the normalization constraint:

$$|A_N(z)| = \sqrt{1 - B_N(z)B_N^*(z)} \tag{2.35}$$

The problem of selecting the most physically meaningful filter $A_N(z)$ was solved by Le Roux (1986), who pointed out that minimum phase $A_N(z)$ yields the pulse that deposits the least amount of RF energy. That choice for the polynomial maximizes its constant term $A_{N,0}$, which from Eq. (2.29) is equivalent to minimizing all the flip angles of the hard pulses and hence the total RF power. Minimum phase polynomials have the property that all of their zeros (roots) lie within the unit circle; that is, if $A_N(z_R) = 0$, then $|z_R| < 1$. Once its magnitude has been determined as in Eq. (2.35), the complete polynomial, including its phase, can be calculated or retrieved with a mathematical tool called a Hilbert transform (named for David Hilbert, 1862–1943, a German mathematician), as explained in Pauly et al. (1991).

Once the minimum phase solution is selected for $A_N(z)$, there are still several inputs to be made to the SLR pulse design. The phase of the filter $B_N(z)$ dropped out of Eq. (2.35), but it is a design choice in the Parks-McClellan algorithm. Minimum, linear, and maximum phases are the most commonly used. In order to reduce the peak RF power, other phase choices (Shinnar 1994), including quadratic phase, can be used instead. The final RF pulse is often referred to according to the phase choice of the filter $B_N(z)$, for example, a minimum phase pulse. Note that the minimum phase solution is always used for $A_N(z)$, regardless of whether minimum, maximum, or linear phase solutions are used for $B_N(z)$.

2.3.2 DESIGN CONSIDERATIONS

The time-bandwidth product (the product of the pulse duration T and the RF bandwidth Δf) is a dimensionless measure of the selectivity of the pulse. A highly selective pulse has an abrupt transition from its passband to its stopband. Because of requirements such as minimum TE or maximum RF power, the desired slice profile might not be attainable with the $T\Delta f$ product available for the pulse. Defining W to be the dimensionless width of the transition band of the response (i.e., $W \times \Delta f$ is the transition width in hertz), then W is determined by the relation (Pauly et al. 1991):

$$T\Delta f\, W = D_\infty \tag{2.36}$$

where D_∞ is a function of the pulse design parameters. Equation (2.36) allows the pulse designer to trade off parameters before the pulse is generated. In Eq. (2.36), D_∞ can be expressed by a simple function (Pauly et al. 1991) of the amount of ripple allowed in the passband and the stopband and of the phase type for the polynomial B. A more selective pulse has a smaller value of W, which can be accomplished either by increasing the time-bandwidth product $T\Delta f$ or by changing the pulse design to decrease D_∞. Increasing the percentage of ripple allowed, particularly in the stopband, is an effective way to decrease D_∞. Also, all other things being equal, minimum and maximum phase RF pulses have smaller values of D_∞ than linear phase pulses. For example, for an excitation pulse with $T\Delta f = 8$, 1.0% passband ripples, and 0.7% ripples in the stopband, $D_\infty = 2.037$ for the linear phase pulse and $D_\infty = 1.628$ for the minimum phase pulse. Therefore, the transition region W is 20% narrower for the minimum phase pulse.

Of the phase types discussed, only linear phase pulses produce a phase dispersion that can be completely rephased with a gradient rephasing lobe. Thus linear phase pulses are commonly used as spatial excitation pulses for 2D pulse sequences. The isodelay (see Section 3.1) of the linear phase pulse is equal to one-half its pulse width:

$$\Delta t_I = \frac{T}{2} \qquad \text{(linear phase)} \tag{2.37}$$

Linear phase pulses also are widely used as slice refocusing pulses, because the phase dispersion accumulated during the first and second halves of the pulse cancel. Figure 2.7 shows an example of a linear phase pulse and its magnetization response.

Minimum phase pulses are useful in a number of applications because they have an isodelay that is less than one-half the pulse width:

$$\Delta t_I < \frac{T}{2} \qquad \text{(minimum phase)} \tag{2.38}$$

and generally the inequality in Eq. (2.38) becomes more extreme as the time-bandwidth product increases. Minimum phase pulses are an excellent choice as excitation pulses for 3D volume gradient echo applications in which it is important to minimize TE. A drawback of minimum phase pulses is that their phase dispersion is a nonlinear function of frequency offset and cannot be completely rephased with a gradient lobe. For 3D acquisitions, however, this is not a serious problem because the phase dispersion of the slice profile is distributed across the entire 3D slab, while intravoxel dephasing is determined by the encoded slice width. In practice, intravoxel phase dispersion due to a minimum phase pulse will rarely result in more than a 1% signal loss if even a minimal number (e.g., 16) of slices are phase encoded. Figure 2.8 shows

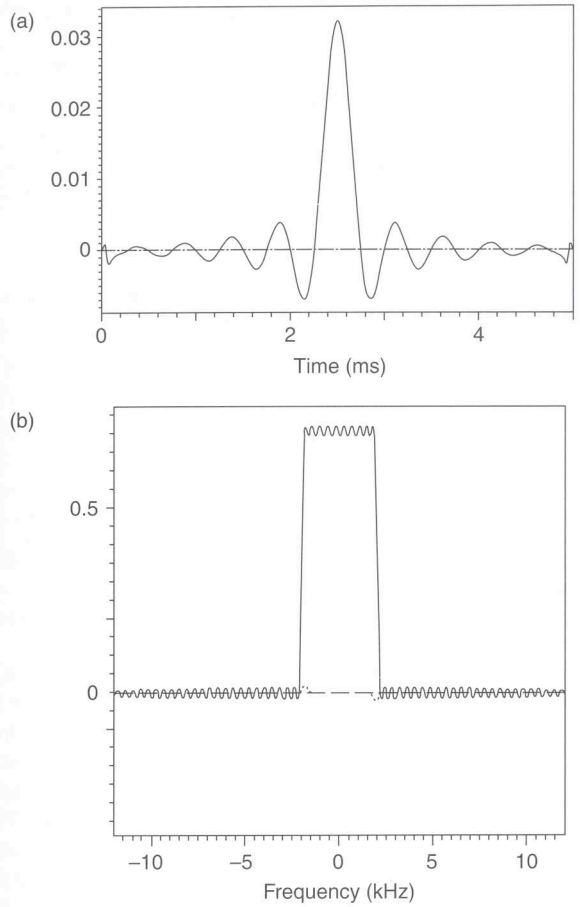

FIGURE 2.7 Linear phase excitation pulse with a time-bandwidth product of 20, a flip angle of 45°, and 2% ripple in both the passband (i.e., in-slice) and the stopband (i.e., out of slice). (a) RF amplitude versus time. (b) M_y and M_x (dotted line) responses. The plot assumes that the optimal rephasing gradient lobe has been applied. Note that M_x is nearly 0 (i.e., the phase across the slice is approximately constant), suggesting that the linear phase introduced during the pulse is effectively rephased by the rephasing gradient lobe.

an example of a minimum phase pulse that could be used as an excitation pulse for a 3D volume acquisition. Because minimum phase pulses have a reduced transition width W compared to linear phase pulses (holding T, Δf, and the ripple percentages constant), a minimum phase pulse also makes a good choice when the phase of the magnetization response is unimportant, such as for inversion pulses.

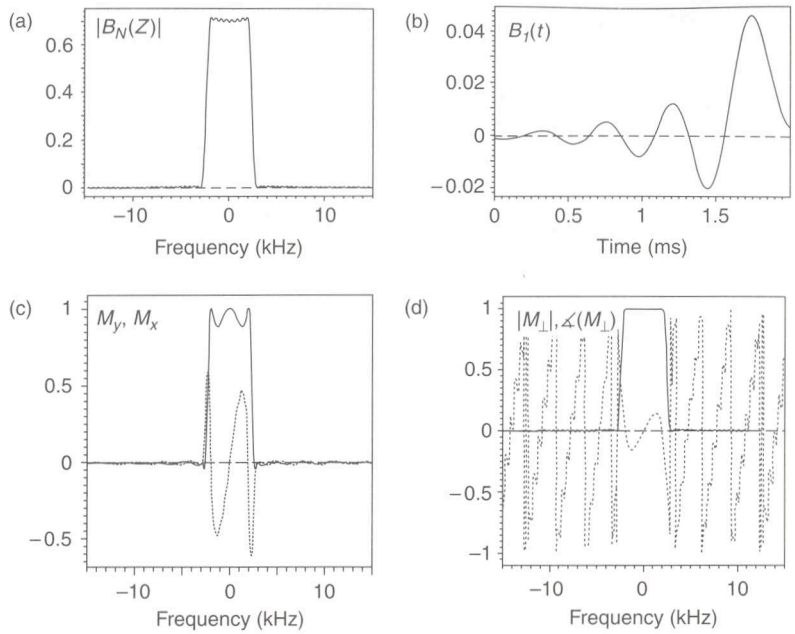

FIGURE 2.8 Minimum phase pulse with a time-bandwidth product of 10, a flip angle of 90°, and 0.5% ripple in the passband and the stopband. (a) The filter (polynomial) $B_N(z)$ plotted versus frequency. (b) The RF amplitude versus time. (c) The M_y and M_x (dotted line) response. (d) Plots of the same response as (c), but this time in terms of the polar instead of Cartesian components. Note from (b) that the isodelay is much less than one-half of the pulse duration ($T = 2$ ms and $\Delta t_I = 288\,\mu$s), and the nonlinear phase is apparent from (c) (real and imaginary) and (d) (modulus and phase). Also the ripples apparent on the filter passband are attenuated in the response (d) compared to (a) because the flip angle is 90°.

Maximum phase pulses can be thought of as time-reversed minimum phase pulses. Consequently their isodelay is greater than one-half their pulse width. Maximum phase pulses are sometimes used for spatial or spectral saturation, where signal dephasing is desirable instead of detrimental.

2.3.3 PRACTICAL CONSIDERATIONS

Pulses designed with the SLR algorithm account for the nonlinearity of the Bloch equations, but only at a single flip angle. For example, if an SLR excitation pulse is designed for a flip angle of 45° but played at a flip angle of 60°, then deviations from the designed profile will begin to emerge. If this is an important consideration, a set of pulses designed for different flip angles

can be stored on the MR scanner. Alternatively, the SLR design could be done in real time when the operator selects the flip angle.

The amount of ripple that is tolerable for the filter $B_N(z)$ depends on the intended function of the pulse. For example, from Table 2.3, a small flip angle excitation pulse response is linearly related to the Cayley-Klein parameter β, and so from Eq. (2.30) it is also proportional to $B_N(z)$. Therefore the amount of ripple in the filter $B_N(z)$ is equal to the amount ripple in the slice profile. For a refocusing pulse with crushers, however, there is a quadratic relationship between β and the response. As shown in Pauly et al. (1991), this implies, for example, that the ripple in the passband of the magnetization response will be four times larger than the ripple in the passband of the filter. SLR pulses are always specified by the desired ripple in the magnetization response, and the corresponding ripple in the filter $B_N(z)$ is calculated according to the type of RF pulse being designed.

The intuitive basis for these types of relations between the ripple in the response and ripple in the filter can be appreciated by considering a 90° (i.e., $\pi/2$) excitation pulse. The magnetization response is proportional to the sine of the flip angle. Near 90°, the ripples in the passband are attenuated because the response is second-order in the ripple amplitude $\Delta\theta$:

$$|M_\perp| = M_0 \sin\left(\frac{\pi}{2} + \Delta\theta\right) = M_0 \cos\Delta\theta = M_0\left(1 - \frac{(\Delta\theta)^2}{2} + \cdots\right) \tag{2.39}$$

Consequently, higher amplitude ripples can be designed into the filter's passband. This effect is illustrated in Fig. 2.8. Quantitative relationships between filter ripple and response ripple for a variety of cases are given in Pauly et al. (1991). It should be noted, however, that if due to B_1 inhomogeneity a pulse intended to be played at 90° (and designed with higher passband ripples) is actually played at 45° over part of the subject, then the passband ripples can be unacceptable in that region.

The amount of stopband ripple that can be tolerated also depends on the specific use of the RF pulse. 3D volume excitation pulses tend to be less forgiving of stopband ripple because the phase encoding process in the slice direction can cause an unwanted signal from the stopband to alias into the desired slice locations (see Example 11.9). If, however, the main issue is whether or not the ripples in the stopband will disturb the z component of off-resonant magnetization (e.g., as with magnetization transfer, chemically selective, or some spatial saturation pulses), then the situation is much more forgiving. The amount of z magnetization that remains undisturbed is proportional to $\cos\Delta\theta$, which from Eq. (2.39) is second order in $\Delta\theta$.

SELECTED REFERENCES

Goldstein, H. 1980. *Classical mechanics*, 2nd ed. Reading: Addison-Wesley.

Jaynes, E. T. 1955. Matrix treatment of nuclear induction. *Phys. Rev.* 98: 1099–1105.

Le Roux, P. 1986. French patent 8610179.

Oppenheim, A. V., and Schaeffer, R. W. 1975. *Digital signal processing*. Englewood Cliffs: Prentice-Hall.

Pauly, J., Le Roux, P., Nishimura, D., and Makovski, A. 1991. Parameter relations for the Shinnar-Le Roux selective excitation pulse design algorithm. *IEEE Trans. Med. Imag.* 10: 53–65.

Shinnar, M. 1994. Reduced power selective excitation RF pulses. *Magn. Reson. Med.* 32: 658–660.

Shinnar, M., Bolinger, L., and Leigh, J. S. 1989a. The synthesis of soft pulses with a specified frequency response. *Magn. Reson. Med.* 12: 88–92.

Shinnar, M., Bolinger, L., and Leigh, J. S. 1989b. The use of finite impulse response filters in pulse design. *Magn. Reson. Med.* 12: 75–87.

Shinnar, M., Eleff, S., Subramanian, H., and Leigh, J. S. 1989. The synthesis of pulse sequences yielding arbitrary magnetization vectors. *Magn. Reson. Med.* 12: 74–80.

Shinnar, M., and Leigh, J. S. 1989. The application of spinors to pulse synthesis and analysis. *Magn. Reson. Med.* 12: 93–98.

Warren, W. S., and Silver, M. E. 1988. The art of pulse crafting: Applications to magnetic resonance and laser spectroscopy. In *Advances in magnetic resonance*, Vol. 12, edited by J. S. Waugh, pp. 247–384. New York: Academic Press.

RELATED SECTIONS

Section 3.1 Excitation Pulses
Section 3.2 Inversion Pulses
Section 3.3 Refocusing Pulses
Section 4.3 Spectrally Selective Pulses

2.4 Variable-Rate Pulses

A one-dimensional spatially selective RF pulse that is played concurrently with a time-varying gradient is called a *variable-rate* (VR) pulse (Conolly et al. 1988, 1991). VR pulses are also known as variable-rate gradient (VRG) pulses or variable-rate selective excitation (VERSE) pulses. One main application of VR pulses is to reduce RF power deposition to the patient, which is accomplished by decreasing the RF amplitude in the vicinity of the peak of the pulse. The peak of the pulse typically contributes the bulk of the power deposition because the contribution to the SAR from the pulse is proportional to the square of its B_1 amplitude. Another application of VR pulses is to play RF concurrently with the gradient ramps, as is commonly done with spatial subpulses in a spatial-spectral pulse (Section 5.4). Playing RF with the ramps makes efficient use of the entire time allotted for the slice-selection gradient lobe, which allows thinner slices or an improvement of the slice profile.

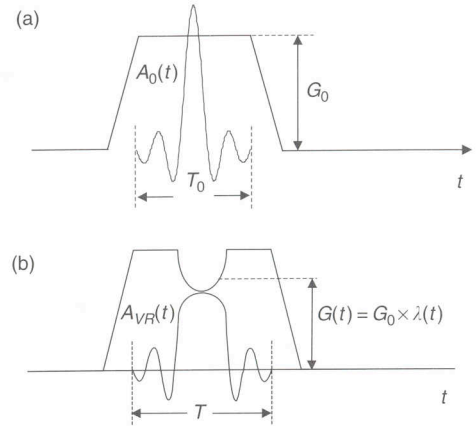

FIGURE 2.9 The variable-rate modification to a SINC RF pulse. The original RF envelope $A_0(t)$ is stretched and attenuated wherever the gradient amplitude is reduced. The gradient amplitude dips according to the function $\lambda(t)$.

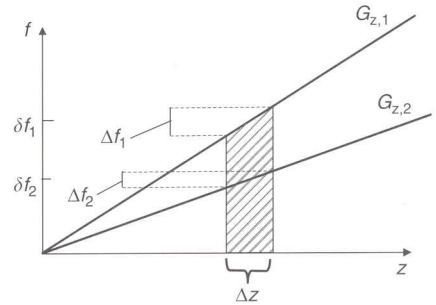

FIGURE 2.10 Whenever the gradient amplitude $G(t)$ is reduced, there is a proportionate reduction in the RF bandwidth Δf and frequency offset δf so that the same slice Δz is produced.

To maintain the nominal flip angle when the RF amplitude is reduced, the VR pulse is proportionately stretched, or time dilated. This in turn reduces the instantaneous RF bandwidth (defined later in Section 2.4) of any portion of the pulse that is stretched. To ensure that the entire VR pulse produces the desired slice profile, the slice-selection gradient amplitude must be proportionately reduced whenever the RF pulse is stretched in order to match the reduced RF bandwidth. Figure 2.9 shows an example of an original and a VR-modified SINC pulse with a concurrent gradient. Figure 2.10 illustrates how the reduced RF bandwidth and reduced gradient amplitude work in concert to maintain the same slice profile.